Photodiagnosis and Photodynamic Therapy 46 (2024) 104047

Contents lists available at ScienceDirect

Photodiagnosis and Photodynamic Therapy

journal homepage: www.elsevier.com/locate/pdpdt

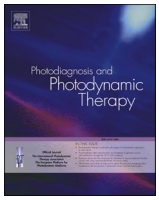

The use of methylene blue to control the tumor oxygenation level

Daria Pominova [a,b,*], Anastasia Ryabova [a,b], Alexey Skobeltsin [a,b], Inessa Markova [b], Kirill Linkov [a], Igor Romanishkin [a]

[a] Prokhorov General Physics Institute of the Russian Academy of Sciences, Moscow, Russia
[b] National Research Nuclear University MEPhI, Moscow, Russia

ARTICLE INFO

Keywords:
Oxygenation
Tumor
Photodynamic therapy
Methylene blue

ABSTRACT

Background: Hypoxia is a characteristic feature of many tumors. It promotes tumor proliferation, metastasis, and invasion and can reduce the effectiveness of many types of cancer treatment.
Objective: The aim of this study was to investigate the pharmacokinetics of methylene blue (MB) and its impact on the tumor oxygenation level at mouse Lewis lung carcinoma (LLC) model using spectroscopic methods.
Approach: The pharmacokinetics of MB were studied qualitatively and quantitatively using video fluorescence imaging and fluorescence spectroscopy. The degree of hemoglobin oxygenation in vivo was examined by calculating hemoglobin optical absorption from the measured diffuse reflectance spectra. The distribution of MB fluorescence and the lifetime of NADH were analyzed using laser scanning microscopy and fluorescence lifetime imaging microscopy (FLIM) to assess cellular metabolism.
Results: After intravenous administration of MB at 10–20 mg/kg, it quickly transitioned in the tumor to a colorless leucomethylene blue, with maximum accumulation in the tumor occurring after 5–10 min. A concentration of 10 mg/kg resulted in a relative increase of the tumor oxygenation level for small tumors (volume 50–75 mm^3) and normal tissue 120 min after the introduction of MB. A shift in tumor metabolism towards oxidative phosphorylation (according to the lifetime of the NADH coenzyme) was measured using FLIM method after intravenous administration of 10 mg/kg of MB. Intravenous administration of MB at 20 mg/kg results in a long-term decrease in oxygenation, which persisted for at least 120 min after the administration and did not return to its initial level.
Conclusions: Administration of MB at 10 mg/kg shown to increase tumor oxygenation level, potentially leading to more effective antitumor therapy. However, at higher doses (20 mg/kg), MB may cause long-term decrease in oxygenation.

1. Introduction

Cancer treatment still remains a significant challenge for both scientists and physicians. Solving this complex problem is hindered by the tumor's gene-expression, independent evolution, metabolism, and high heterogeneity of tumors [1,2], as well as a large number of interrelated factors that lead to changes in the tumor microenvironment [3–5]. As result, the tumor microenvironment possesses distinct physiological traits compared to healthy tissue.

Cancer cells exhibit active growth and prefer to produce ATP through the glycolytic system for biomass production, known as aerobic glycolysis, in addition to oxidative phosphorylation, even when sufficient oxygen is present in the tissue [6]. This increased glycolytic activity results in high lactate production, which plays a critical role in signaling, regulation of cancer immunity, and immunosuppression [7,8]. The accumulation of lactate in tumors indicates a rise in NADH levels compared to NAD^+. Cancer cells have been found to have a higher NADH/NAD^+ redox ratio than normal cells [9–11], where the ratio of NAD^+ to NADH is balanced in favor of NAD^+. In cancer cell mitochondria, NADH is used to maintain high NADPH levels, which is essential for the production of scavenging enzymes, regulation of reactive oxygen species (ROS) levels and tumor defense against oxidative stress and cell death [12].

Accelerated tumor growth results in chronic hypoxia as oxygen consumption exceeds its supply. This causes a gradual decrease in tumor oxygenation as the distance from the tumor-associated vasculature increases [13]. In addition, acute or perfusion-related hypoxia may occur due to an irregular or dilated vascular network in tumor or vascular occlusion caused by tumor cell aggregates [14,15]. Normal tissue oxygen levels range from 10 to 80 mmHg, while most tumor tissues have

* Corresponding author.

https://doi.org/10.1016/j.pdpdt.2024.104047
Received 31 October 2023; Received in revised form 12 February 2024; Accepted 8 March 2024
Available online 19 March 2024

levels below 5 mmHg [16]. Poor patient outcomes are associated with the expression of the hypoxia-inducible factor 1 (HIF-1) [17–19]. Hypoxia promotes tumor proliferation, metastasis, and invasion, as well as resistance to cancer treatments [20–22], and can reduce the effectiveness of all types of cancer therapies, including radiotherapy, chemotherapy [23–25], and photodynamic therapy [26].

The aim of developing new therapeutic modalities is often to increase the oxygen content in tumors, with the goal of enhancing therapy efficacy. Recently proposed strategies [26] for addressing tumor hypoxia include direct delivery of exogenous oxygen to the tumor or generation of oxygen in situ [20,25,27], reducing tumor cellular oxygen consumption by inhibiting respiration [28,29], normalizing tumor vasculature, or disrupting tumor extracellular matrix [30–32], and inhibiting the HIF-1 signaling pathway [33]. Additionally, the oxygen-independent Type-I PDT is also discussed as an alternative strategy [34,35].

One interesting approach is the development and study of nanozymes — nanostructures that mimic the catalytic properties of natural enzymes. Most nanozymes can catalyze the degradation of peroxides and are actively used to generate oxygen in situ [36–38]. There is also growing interest in developing nanozymes for other cofactors involved in cellular metabolic redox reactions, such as NADH/NAD [39]. Well-known redox dyes, such as methylene blue (MB), can be used for the same purposes.

MB is a heterocyclic aromatic phenothiazine dye discovered by Heinrich Caro in 1876. Early research on methylene blue dates back to the 1930s, when the idea was proposed that MB could increase oxygen consumption by tissues prone to aerobic glycolysis, particularly tumors, and also to restore oxygen consumption after cyanide poisoning [40]. The effect of MB was proposed to be proportional to the enzymatic capacity of tissues, and the catalytic properties of MB in relation to tumors are due to its interaction with lactic acid produced as a result of aerobic glycolysis. MB has been actively studied as an antidote for cyanide poisoning [41–44], but, after the advent of other antidotes, research was discontinued for quite some time.

MB is currently being actively researched and widely used clinically, both for fluorescence-based intraoperative imaging [45,46] and as a PDT agent [47–52]. Its catalytic properties find application in the treatment of methemoglobinemia [53,54] and lactoacidosis [55], as well as an antidote for carbon monoxide [44] or cyanide poisoning [42]. During interaction with cell membranes, dimerization of MB promotes electron transfer reactions leading to the generation of reactive oxygen species and Type-I PDT [56,57].

A more detailed understanding of the metabolic pathways of tumor development generates interest in redox dyes. Modern methods allow a more detailed analysis of the effect of MB on metabolism, both at the cellular level and on the tumor as a whole. It is well-known that MB is capable of exhibiting cyclic redox properties both in vitro and in vivo [58,59]. The in vivo cyclic activity is caused by the interaction with molecules found in the cytoplasm or mitochondria, such as NADH [60,61], FADH or reduced glutathione [58]. This leads to the rapid reduction of MB to its colorless form, leucomethylene blue (LMB), in the absence of oxygen [62]. Oxygen and molecules with high oxidation potential, can then re-oxidize LMB to MB, creating a cyclic electron donor-acceptor pair [59,63,64].

The effects of MB/LMB pair can vary significantly depending on the MB concentration and the redox state of its immediate environment. For instance, low concentrations of MB are used to treat methemoglobiemia, while high concentrations act as an electron acceptor [59] and may lead to methemoglobiemia. The cycling between the oxidized and reduced forms of MB, which facilitates electron transport in the mitochondria and enhances the ATP production through the oxidative phosphorylation at nM or low μM concentrations of MB (up to 10 μM) [65–67]. Positive effects have been reported at high concentrations up to 60 μM [68].

Most of the studies on the influence of MB on cell and tissue metabolism have been conducted in cell cultures, animals or *ex vivo* organs. These studies have established important patterns of MB influence, which depend on the concentration of MB and the redox state of the microenvironment [69,70]. However, due to the large number of interacting factors, it is not always possible to model the entire set of experimental factors in vitro and *ex vivo*. Therefore, in this article, we used modern spectroscopic methods to study the accumulation of MB in normal tissues and in tumors of laboratory animals in vivo and to investigate the effect of MB on oxygenation.

2. Materials and methods

2.1. Tumor model in vivo

Male BALB/c mice weighting 25–30 g and aged 8–10 weeks were used in experiments conducted at the N.N. Blokhin National Medical Research Center of Oncology. The mice were obtained from the Pushchino nursery (Russia) and were in standard cages at a temperature of 21℃ with a 12-hour light-dark cycle. They were given ad libitum access to standard laboratory feed and water. Tumor grafting was performed by intramuscular injection of 50 μl of a 15 % C57LB strain Lewis lung carcinoma (LLC) tumor cell suspension in Hanks' Balanced Salt Solution the into the right hind leg. Tumor growth was assessed at 6, 8, 10, and 14 days post-injection by measuring two perpendicular diameters of each tumor with calipers. The tumor size was determined by direct measurement of its dimensions, and the volume was calculated using the formula: $V = 0.5\ (L \times W^2)$, where V — volume, L — length and W — width.

Experiments were conducted on 14th day after the injection of LLC cells. The animals were administered a commercially available photosensitizer Methylene Blue (MB, Samaramedprom, Russia). The 200 μl of 1 % aqueous solution of MB in saline (based on a total dose of 10 and 20 mg/kg (0.031 mM and 0.062 mM) in an animal) were administered intravenously into the tail vein under fluorescence control.

The mice were divided into four groups based on tumor size (small and large tumor, corresponding to 50–75 mm^3 and 100–150 mm^3, respectively) and MB concentration (total dose of 10 and 20 mg/kg). Each group consisted of three mice. Oxygenation measurements were taken at three locations in both tumor and normal muscle tissue for 30 s for each mouse. Fluorescence measurements were also taken at three locations in both tumor and normal muscle tissue. After this, the data was averaged and STD was calculated.

2.2. Video fluorescence imaging

Fluorescence was excited using 660 nm laser radiation and detected by a black-and-white MQ013RG-ON camera (Ximea, Korea) sensitive to near-infrared wavelengths and equipped with a 700–750 nm bandpass optical filter. The fluorescence signal was recorded as the image brightness for 5 min following the administration of MB solution in both tumor and normal tissue.

2.3. Diffuse-reflected fluorescence spectroscopy

The accumulation of MB was measured spectroscopically in both tumor and normal tissue using a LESA-01-Biospec fiber-optic spectrometer (Biospec, Russia) with fiber-optic probe. The device can measure fluorescence spectra in the 350–1000 nm wavelength range with a 3 nm resolution and an adjustable exposure between 20 and 500 ms. The probe consisted of a central illuminating fiber that provided laser radiation to excite the tissue and six peripheral fibers that collected the scattered and fluorescence radiation. An He-Ne laser emitting at 632.8 nm was utilized for exciting MB fluorescence. The power of laser radiation at the fiber output was 5 mW. An optical filter was installed at the spectrometer entrance to reduce laser radiation, allowing for the observation of component backscattered by tissue within the same

dynamic range as fluorescence radiation.

The concentration of the photosensitizer in the tissues was calculated by measuring integral intensity of fluorescence. A calibration was carried out using optical phantoms that replicate the scattering and absorption properties of biological tissues. These phantoms contained MB at concentrations ranging from 0 to 5 mg/kg in a scattering medium of 1 % Intralipid fat emulsion (Fresenius Kabi LLC, USA) in a test tube. The fluorescence index was calculated for each optical phantom by dividing the area under the MB fluorescence peak by the area under the scattered laser radiation peak. The fluorescence indices of the optical phantoms were used to construct a calibration curve. Both the tissue fluorescence index and MB concentration in optical phantoms were determined under identical external conditions. Measurements were taken before MB administration and at time intervals ranging from 5 to 120 min after the administration. At each time point, three measurements were taken for each animal. For statistical analysis of the obtained data, the Shapiro-Wilk test was used to determine whether the sample followed a normal distribution. After confirming the normal distribution, we performed a two-sample *t*-test to evaluate the difference between the values at each measured time point and the value at zero (before drug administration), as well as between time points for trend analysis.

2.4. Measurement of hemoglobin oxygenation level

The degree of hemoglobin oxygenation in vivo was examined using a hemoglobin optical absorption method [71]. A halogen lamp with a fiber-optic output functioned as the broadband light source, while LESA-01-Biospec fiber-optic spectrometer registered the diffuse reflectance spectra. The hemoglobin concentration was derived from the absorption spectrum. The degree of hemoglobin oxygenation was calculated as the ratio of oxygenated hemoglobin absorption to total hemoglobin absorption. For statistical analysis of the obtained data, the Shapiro-Wilk test was used to determine whether the sample followed a normal distribution. Since the obtained data did not follow a normal distribution, we performed Wilcoxon signed rank test to check the data for a significant difference between two population medians.

2.5. Fluorescence microscopy and fluorescence lifetime imaging microscopy (FLIM)

Mice were euthanized immediately and 5 min after MB injection. A mouse with a tumor without MB administration was used as a control. Tumors, subcutaneous tissue, skin, and muscle were excised en bloc and frozen. Sections were cut at a thickness of 50 μm using a Microm HM 560 Cryostat (Thermo Scientific, Waltham, MA, USA) and processed for laser scanning fluorescence microscopy and FLIM procedures to analyze the accumulation of MB within individual cells. The sections were placed in saline under a coverslip and examined immediately.

The fluorescence spectra and lifetime images of autofluorescence and MB fluorescence were recorded using a laser scanning confocal microscope LSM-710-NLO (Carl Zeiss AG, Oberkochen, Germany). The spectrally resolved images were acquired under simultaneous 488 nm and 633 nm laser excitation in lambda mode with 32-channel GaAsP detector in the 450–740 nm spectral range. The average autofluorescence level was determined from tumor sections of mice without MB administration for subtraction from the spectra of tumor sections of mice with MB administration. Using the same image acquisition parameters, images of aqueous MB solutions were obtained to assess the level of MB concentration in tumor sections. Time-resolved images of autofluorescence and MB fluorescence were recorded under two-photon 740 nm excitation with a Chameleon Ultra II femtosecond laser (Coherent, Saxonburg, Pennsylvania, USA), with a pulse width of 140 fs and a repetition rate of 80 MHz. Optical bandpass filters FB450–40 (Thorlabs, Newton New Hersey, USA) and BP 640/30 (Carl Zeiss AG, Oberkochen, Germany) were used to isolate fluorescence signals from NADH and MB, respectively. Time-resolved fluorescence images were processed using SPCImage 8.0 software (Becker & Hickl GmbH, Berlin, Germany). In calculating the NADH a_1/a_2 metabolic index, kinetics were approximated using fixed lifetimes: $\tau_1 = 0.4$ ns, $\tau_2 = 2.5$ ns [72].

For statistical analysis of the obtained data, the Shapiro-Wilk test was used to determine whether the sample followed a normal distribution. After confirming the normal distribution, we performed a two-sample *t*-test to evaluate the difference between the NADH lifetime values for tumors after MB injection with value for control tumor without MB.

3. Results

The results of a qualitative study of the MB pharmacokinetics using the video fluorescence method are shown in Fig. 1.

Immediately after intravenous MB administration an intense fluorescent signal was observed in both tumor and normal tissue. In normal tissue, the signal remains at a constant level until the end of the measurement. In tumors, the signal decays rapidly: for small tumors, the signal decays to 20 % of the initial brightness after approximately 50 s. For large tumors, the signal decays even more rapidly, reaching 20 % of the initial brightness in 20 s. The signal then slowly increases to 30 % of the initial brightness. It should be noted that, after 15 s, vessels in the tumor are clearly visualized; after 300 s, the staining is more diffuse, which may indicate the accumulation of MB in different tumor compartments.

The results of a quantitative study of MB pharmacokinetics using fluorescence spectroscopy are presented in Fig. 2.

In normal tissues, the maximum of MB accumulation was observed at 5–10 min after injection, after which the fluorescence intensity began to decrease. At 10 mg/kg administered dose, statistically significant differences in accumulation were observed between the 5- and 120-minute time points. The rate of signal decrease was higher at a higher concentration of MB (20 mg/kg), statistically significant differences in accumulation were observed already between the 5- and 10-minute time points, the trend of decreasing concentration continued up to 120 min. A similar trend was observed in small tumors. The maximum accumulation of MB observed after 10 min for small tumors was 0.11 ± 0.02 mg/kg at a dose of 10 mg/kg and 0.16 ± 0.03 mg/kg at a dose of 20 mg/kg. For large tumors, the measured MB concentration was significantly lower (the maximum accumulation was 0.05 ± 0.01 mg/kg at a dose of 10 mg/kg and 0.09 ± 0.01 mg/kg at a dose of 20 mg/kg) and the error of calculated concentration is higher, no statistically significant difference was found to determine the trend of MB accumulation. This may be due to both the significant heterogeneity of large tumors and poorer blood supply, as well as the transition of part of the MB to a colorless LMB form under hypoxic conditions.

The results of the oxygenation study of normal tissues and tumors are shown in Fig. 3.

In normal tissues, a decrease in the oxygenation level was observed at short time intervals, 5 – 10 min, corresponding to the maximum accumulation of MB. With increasing time, a reverse increase in the level of oxygenation is observed, and after administration of 10 mg/kg, the level of oxygenation after 2 h exceeds the initial one ($p < 0.01$). Intravenous injection of 20 mg/kg MB leads to a decrease in oxygenation of normal tissues over the entire time interval studied; after 120 min, oxygenation is still below the initial level ($p < 0.01$).

In small tumors, intravenous administration of MB at a concentration of 10 mg/kg results in a short-term decrease in oxygenation after 5–10 min. However, after this initial decrease, there is a subsequent increase in oxygenation levels, with oxygenation after 120 min exceeding the initial value ($p < 0.01$). Intravenous administration of MB at a concentration of 20 mg/kg leads to a long-term decrease in oxygenation; 120 min after administration, the level of tumor oxygenation still does not reach the initial value ($p < 0.01$).

In large tumors, intravenous administration of MB at a concentration of 10 mg/kg does not lead to statistically significant changes in oxygenation Intravenous administration of MB at a concentration of 20

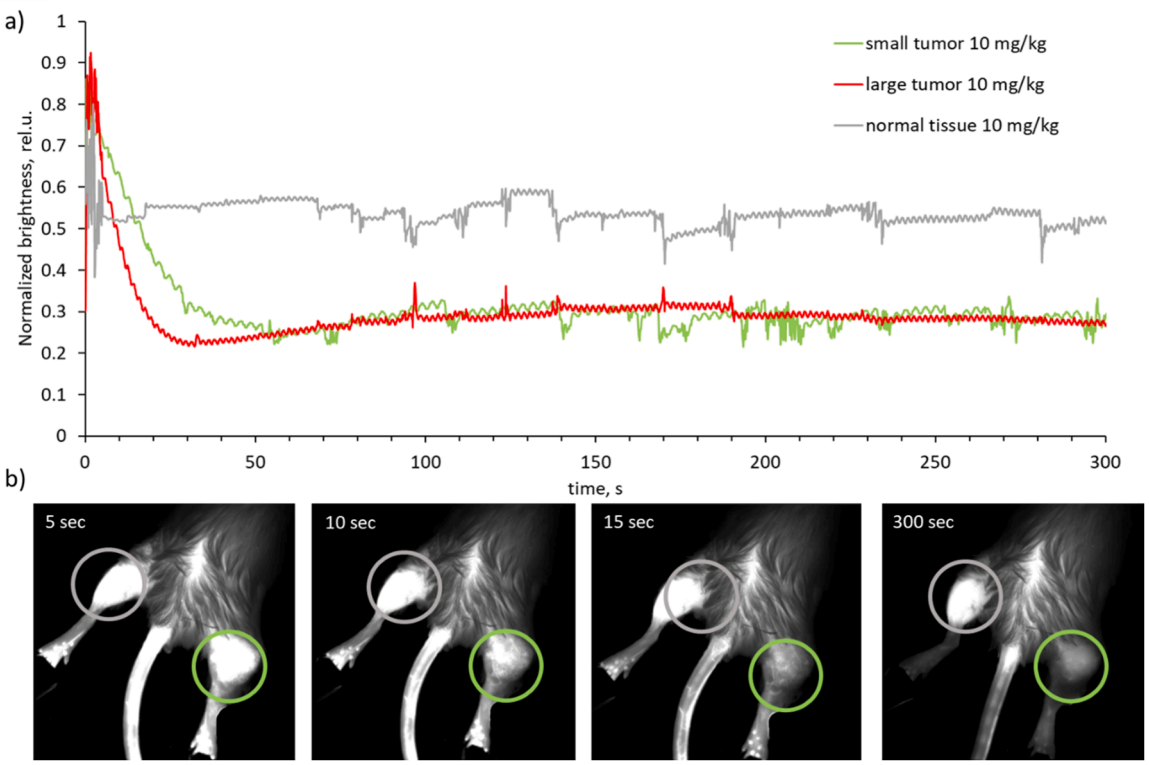

Fig. 1. a) Normalized MB fluorescence brightness after intravenous administration in mice observed in normal leg (left hind leg), large and small tumors (right hind leg, volume 100–150 and 50–75 mm^3, respectively) over time. b) Frames of fluorescence images of mouse legs, healthy (gray circle) and with a grafted tumor (green circle) over time after intravenous administration of MB.

mg/kg causes a long-term decrease in oxygenation in large tumors, after 120 min the level of tumor oxygenation still does not reach the initial value ($p < 0.05$).

The obtained dependencies indicate that small tumors exhibit faster and most severe decrease in oxygenation, while large tumors experience less pronounced decline. At low dose of MB, the oxygenation level increases above the initial level for small tumors and normal tissue. Conversely, at high dose of MB, the oxygenation level remains below its initial value throughout the entire time of the experiment.

Cryosections of tumors were examined using laser scanning microscopy and FLIM. The distribution of MB fluorescence and the lifetime of NADH were analyzed to assess cellular metabolism. The MB fluorescence was detected on tumor cryosections only for the animal that was euthanized immediately after intravenous administration of MB, Fig. 4. Five minutes after intravenous injection of MB into the tumors, no traces of MB fluorescence could be detected.

The mean fluorescence lifetimes of NADH (τ NADH) measured by FLIM and averaged across tumor regions such as healthy muscle, tumor border, deep tumor core are given in Table 1.

In mice with MB in tumor, NADH shows a shift towards longer fluorescence lifetimes compared to control, even when no MB was detected. This increase in NADH fluorescence lifetime can be interpreted as a shift in metabolism towards oxidative phosphorylation [73].

4. Discussion

The LLC model is commonly used to evaluate the efficacy of new drugs, particularly those with antiangiogenic properties [74,75]. LLC grows rapidly, forming a heterotopic graft. The metabolic phenotype of lung cancer cells is characterized by increased glucose uptake and glycolytic activity. Thus, in the selected model, the presence of a microenvironment that is characteristic of a rapidly proliferating tumor (excess of lactate [7], NADH [11], and hypoxia [16]) is expected. This is also confirmed by experimental results. Tumor oxygenation, measured before MB administration, is significantly lower than that of normal tissue (about 75 %) and amounts to 60 % and 50 % for small and large tumors, respectively.

After intravenous administration, MB is quickly distributed throughout all organs and tissues due to the small size of its molecules [76]. Since the intensity of the fluorescent signal in tumors begins to decrease almost immediately after intravenous injection, and decreases more rapidly in large tumors, Fig. 1a), we assume that this is not only due to the blood flow and the accumulation/removal of MB from tissues, but also due to its transition to the LMB when interacting with coenzymes in the tumor. The constant level of fluorescence intensity in normal tissues over a 300-second time period confirms this assumption. Even if the transition to LMB occurs in normal tissues, rapid reoxidation into the MB is likely due to the good oxygen supply. Such trend was shown for MB in closed system when interacting with NADH [61] — under anaerobic condition a rapid transition of MB to LMB occurs, while under aerobic condition no changes in MB absorption were observed, however a decrease in the amount of NADH was observed. We assume that the interaction with NADH leads to changes in oxygenation.

The interaction between MB and NADH in both tumor and normal tissue, on the one hand, is determined by the speed of blood flow, which affects the delivery of MB to the tumor, and on the other hand, by the amount of NADH that acts as a reducing agent of MB to LMB and oxygen, which acts as an oxidizer of LMB to MB.

The concentration of MB in large tumors, as determined by spectroscopic methods, does not exceed 0.1 mg/kg, Fig. 2. The maximum accumulation was 0.05 ± 0.01 mg/kg at an administration dose of 10 mg/kg and 0.09 ± 0.01 mg/kg at an administration dose of 20 mg/kg, compared to 0.11 ± 0.02 mg/kg and 0.16 ± 0.03 mg/kg for small tumors, respectively. This may be due to poor accumulation resulting from insufficient blood supply and hypoxia in large tumors, which causes the transition of MB to LMB. At the same time, at a concentration of 10 mg/

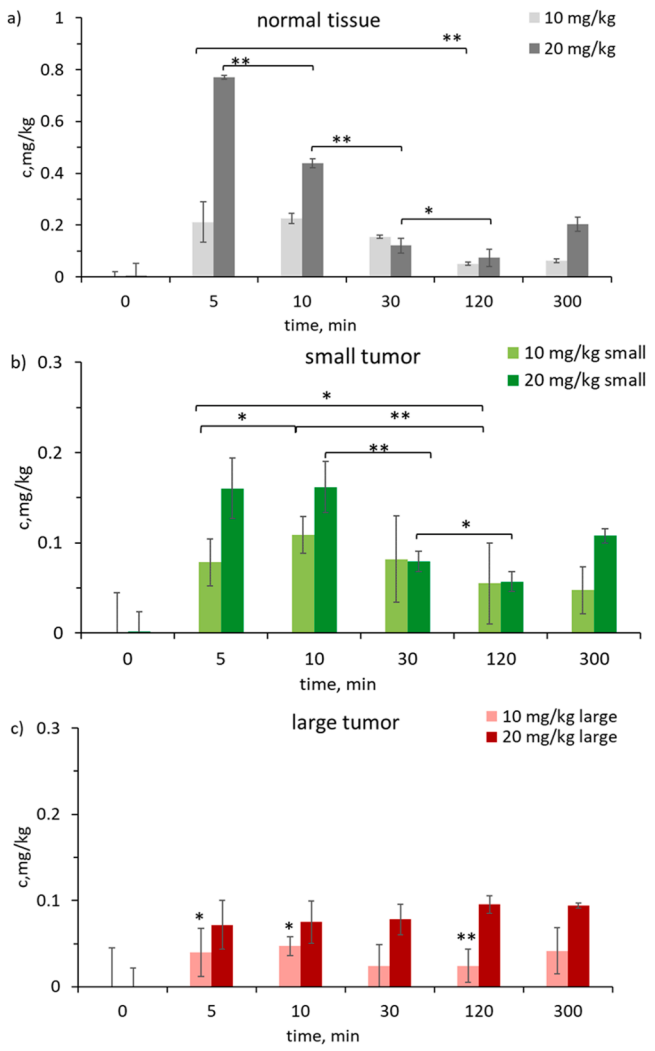

Fig. 2. Pharmacokinetics of MB after intravenous administration at a dose of 10 and 20 mg/kg in normal tissue (a) small (volume 50–75 mm^3) and (b) and large (volume 100–150 mm^3) (c) tumors, measured using fluorescence spectroscopy. For (c) time points statistically significantly different from the concentration at zero (before MB administration) are marked (*$p < 0.05$, **$p < 0.01$).

kg, MB has a weak effect on the oxygenation of large tumors, with the measured changes in oxygenation not being statistically significant, Fig. 3.

Based on this, we assume that slow blood flow in large tumors may be the reason for the ineffective accumulation of MB and its minor effect on the oxygenation in large tumors, despite the high NADH content and rapid transition of MB to LMB, Fig. 1a).

When comparing the effect of MB on the oxygenation of small tumors and normal tissues, Fig. 3, it is evident that despite the lower concentration of MB in the tumor compared to normal tissue, the effect on oxygenation is comparable and demonstrates the same trend. The transition from MB to LMB can result in underestimation of the concentration measured in the tumor by spectroscopic methods. Additionally, a higher amount of NADH in the tumor promotes more effective catalytic reaction.

The effect of MB on oxygenation is dependent in the dose. Low concentrations (10 mg/kg, equivalent to 30 μM) resulted in a rapid decrease followed by an increase to a level higher than the initial.

Interestingly, the observed effect very quickly leads to a shift in metabolism towards oxidative phosphorylation. An increase in NADH lifetime was observed in animals euthanized immediately after the

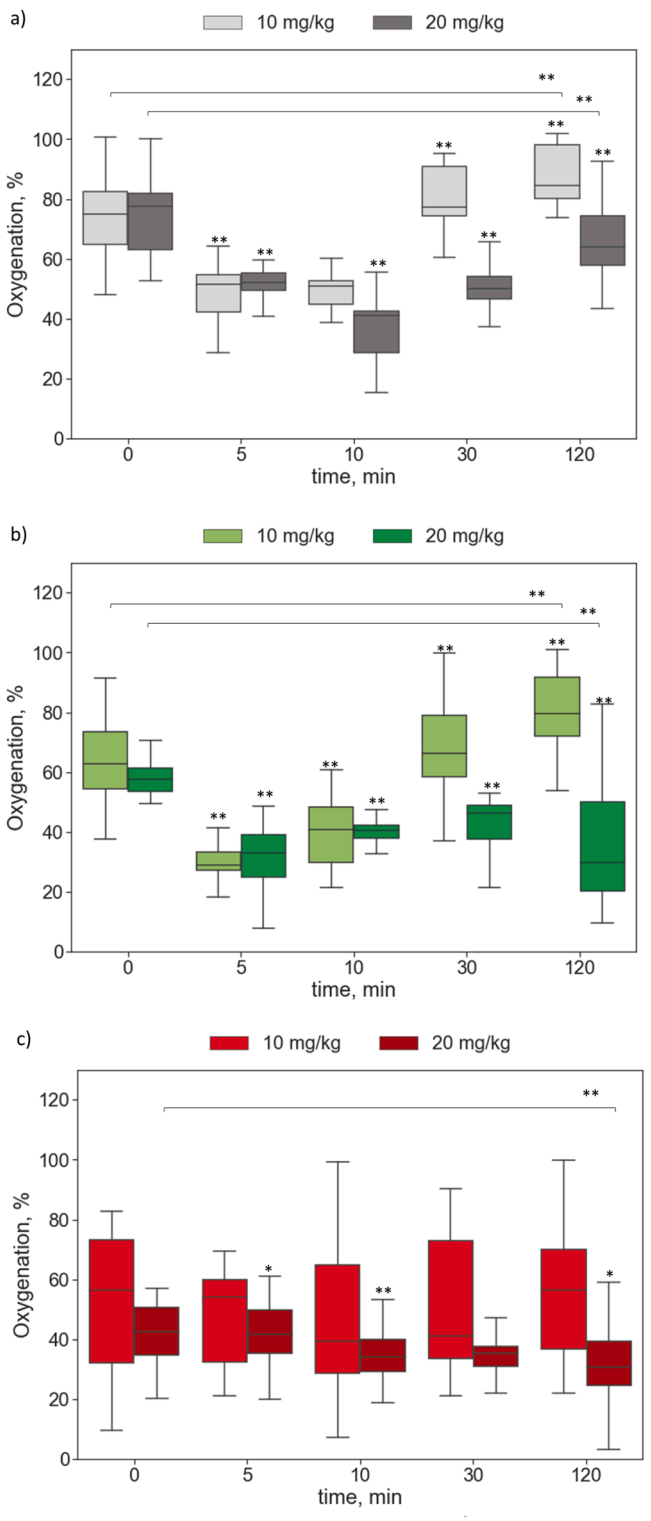

Fig. 3. Oxygenation of normal tissues (a) small (volume 50–75 mm^3) (b) and large (volume 100–150 mm^3) (c) tumors, measured by hemoglobin absorption. To evaluate statistically significantly difference, the values at each measured time point were compared with the value at the previous time point. **$p < 0.01$.

administration of MB. In animals euthanized 5 min after the administration of MB the effect intensifies.

High concentrations (20 mg/kg, equivalent to 60 μM) of MB negatively affected the oxygenation in both tumors and normal tissues. In case of large tumors it resulted in a long-term decrease in oxygenation.

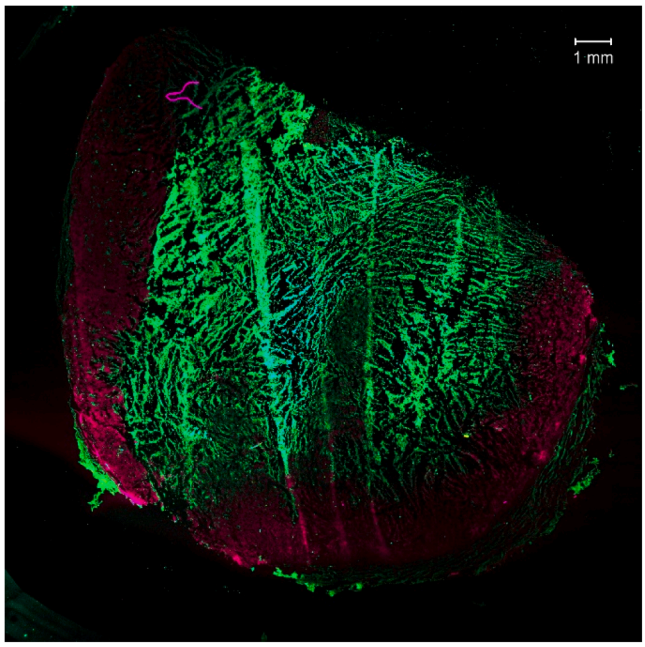

Fig. 4. Fluorescence image of a tumor cryosection from a mouse euthanized immediately after MB administration. Red color corresponds to the MB fluorescence wavelength range, green — autofluorescence.

Table 1
Results of tumor sections examination with fluorescence and time-resolved microscopy.

sample	region	MB fluorescence level	τ NADH [ns] (μ±σ)
control without MB	tumor, about 2 mm from surface	NA	0.86 ± 0.14
euthanized immediately after MB administration	tumor surface	0.2 mg/kg	1.00 ± 0.13*
	tumor, about 2 mm from surface	NA	0.59 ± 0.10*
	tumor, more than 2 mm from surface	NA	0.75 ± 0.09
euthanized in 5 min after MB administration	tumor surface	NA	1.16 ± 0.20*
	tumor, more than 2 mm from surface	NA	1.15 ± 0.22*

Note: NA – less than detectable.
* indicates $p < 0.05$, comparison using two sample *t*-test with value for control without MB.

This indirectly confirms our assumption that blood flow plays a role in the low accumulation of MB in large tumors.

Similar concentration-dependent effects have also been reported in the literature. Cases of desaturation of patient tissue with oxygen, in combination with a concomitant drop in the partial pressure of oxygen in the alveoli after MB administration, have been reported [77–79]. The concentration ranges resulting in a shift between the positive and negative effects of MB are consistent with the literature data. [65–68].

5. Conclusion

It was demonstrated that MB therapy enhances tumor oxygenation levels, which contributes to more effective antitumor therapy.

For low concentrations of MB (10 mg/kg, equivalent to 30 μM), the oxygenation level increased in small tumors and normal tissue 120 min after the MB introduction. We suggest that even lower concentrations of MB may have a more significant effect on tumor oxygenation. Along with an increase in oxygenation, there is also a shift in metabolism towards oxidative phosphorylation. It is important to note that the observed effects are highly dose-dependent. For high concentrations of MB (20 mg/kg, equivalent to 60 μM), a negative effect on the oxygenation of both tumors and normal tissues was observed.

Institutional review board statement

All animal experiments were performed in accordance with European and Russian national guidelines for animal experimentation and were approved by the ethics review committee of the N.N. Blokhin NMRCO (reference number 2017-034, 17 June 2017).

Informed consent statement

Not applicable.

CRediT authorship contribution statement

Daria Pominova: Writing – review & editing, Writing – original draft, Visualization, Validation, Resources, Project administration, Methodology, Investigation, Conceptualization. **Anastasia Ryabova:** Writing – review & editing, Validation, Methodology, Investigation. **Alexey Skobeltsin:** Methodology, Investigation. **Inessa Markova:** Visualization, Investigation. **Kirill Linkov:** Writing – review & editing, Methodology. **Igor Romanishkin:** Writing – review & editing, Visualization, Validation, Software, Methodology, Formal analysis.

Declaration of competing interest

The authors declare no conflict of interest. The funders had no role in the design of the study; in the collection, analyses, or interpretation of data; in the writing of the manuscript; or in the decision to publish the results.

Funding

The study was funded by a grant from the Russian Science Foundation (project N 22-72-10117).

Acknowledgments

The authors are grateful to Saida Karshieva, a staff member of the N. N. Blokhin NMRCO for help with the in vivo experiments.

References

[1] I. Dagogo-Jack, A.T. Shaw, Tumour heterogeneity and resistance to cancer therapies, Nat. Rev. Clin. Oncol. 15 (2018) 81–94, https://doi.org/10.1038/nrclinonc.2017.166.
[2] P.L. Bedard, A.R. Hansen, M.J. Ratain, L.L. Siu, Tumour heterogeneity in the clinic, Nature 501 (2013) 355–364, https://doi.org/10.1038/nature12627.
[3] E. Pranzini, E. Pardella, P. Paoli, S.-M. Fendt, M.L. Taddei, Metabolic reprogramming in anticancer drug resistance: a focus on amino acids, Trends Cancer 7 (2021) 682–699, https://doi.org/10.1016/j.trecan.2021.02.004.
[4] S.K. Biswas, A. Mantovani, Macrophage plasticity and interaction with lymphocyte subsets: cancer as a paradigm, Nat. Immunol. 11 (2010) 889–896, https://doi.org/10.1038/ni.1937.
[5] A.A. Alizadeh, V. Aranda, A. Bardelli, C. Blanpain, C. Bock, C. Borowski, C. Caldas, A. Califano, M. Doherty, M. Elsner, M. Esteller, R. Fitzgerald, J.O. Korbel, P. Lichter, C.E. Mason, N. Navin, D. Pe'er, K. Polyak, C.W.M. Roberts, L. Siu, A. Snyder, H. Stower, C. Swanton, R.G.W. Verhaak, J.C. Zenklusen, J. Zuber, J. Zucman-Rossi, Toward understanding and exploiting tumor heterogeneity, Nat. Med. 21 (2015) 846–853, https://doi.org/10.1038/nm.3915.
[6] M.G. Vander Heiden, L.C. Cantley, C.B. Thompson, Understanding the Warburg effect: the metabolic requirements of cell proliferation, Science 324 (2009) 1029–1033, https://doi.org/10.1126/science.1160809.
[7] O.R. Colegio, N.-Q. Chu, A.L. Szabo, T. Chu, A.M. Rhebergen, V. Jairam, N. Cyrus, C.E. Brokowski, S.C. Eisenbarth, G.M. Phillips, G.W. Cline, A.J. Phillips, R. Medzhitov, Functional polarization of tumour-associated macrophages by

tumour-derived lactic acid, Nature 513 (2014) 559–563, https://doi.org/10.1038/nature13490.
[8] V. Huber, C. Camisaschi, A. Berzi, S. Ferro, L. Lugini, T. Triulzi, A. Tuccitto, E. Tagliabue, C. Castelli, L. Rivoltini, Cancer acidity: an ultimate frontier of tumor immune escape and a novel target of immunomodulation, Semin. Cancer Biol. 43 (2017) 74–89, https://doi.org/10.1016/j.semcancer.2017.03.001.
[9] R.J. DeBerardinis, J.J. Lum, G. Hatzivassiliou, C.B. Thompson, The biology of cancer: metabolic reprogramming fuels cell growth and proliferation, Cell Metab. 7 (2008) 11–20, https://doi.org/10.1016/j.cmet.2007.10.002.
[10] A.A. Heikal, Intracellular coenzymes as natural biomarkers for metabolic activities and mitochondrial anomalies, Biomark. Med. 4 (2010) 241–263, https://doi.org/10.2217/bmm.10.1.
[11] A. Chiarugi, C. Dölle, R. Felici, M. Ziegler, The NAD metabolome — a key determinant of cancer cell biology, Nat. Rev. Cancer 12 (2012) 741–752, https://doi.org/10.1038/nrc3340.
[12] F. Ciccarese, V. Ciminale, Escaping death: mitochondrial redox homeostasis in cancer cells, Front. Oncol. 7 (2017) 117, https://doi.org/10.3389/fonc.2017.00117.
[13] B. Muz, P. De La Puente, F. Azab, A.K. Azab, The role of hypoxia in cancer progression, angiogenesis, metastasis, and resistance to therapy, HP 83 (2015), https://doi.org/10.2147/HP.S93413.
[14] P.N. Span, J. Bussink, Biology of Hypoxia, Semin. Nucl. Med. 45 (2015) 101–109, https://doi.org/10.1053/j.semnuclmed.2014.10.002.
[15] P. Vaupel, L. Harrison, Tumor hypoxia: causative factors, compensatory mechanisms, and cellular response, Oncologist. 9 (2004) 4–9, https://doi.org/10.1634/theoncologist.9-90005-4.
[16] K.R. Luoto, R. Kumareswaran, R.G. Bristow, Tumor hypoxia as a driving force in genetic instability, Genome Integr. 4 (2013), https://doi.org/10.1186/2041-9414-4-5.
[17] G.L. Semenza, Hypoxia-inducible factors in physiology and medicine, Cell 148 (2012) 399–408, https://doi.org/10.1016/j.cell.2012.01.021.
[18] E.L. LaGory, A.J. Giaccia, The ever-expanding role of HIF in tumour and stromal biology, Nat. Cell Biol. 18 (2016) 356–365, https://doi.org/10.1038/ncb3330.
[19] E.B. Rankin, A.J. Giaccia, Hypoxic control of metastasis, Science 352 (2016) 175–180, https://doi.org/10.1126/science.aaf4405.
[20] A. Sahu, I. Kwon, G. Tae, Improving cancer therapy through the nanomaterials-assisted alleviation of hypoxia, Biomaterials 228 (2020) 119578, https://doi.org/10.1016/j.biomaterials.2019.119578.
[21] N. Chan, M. Koritzinsky, H. Zhao, R. Bindra, P.M. Glazer, S. Powell, A. Belmaaza, B. Wouters, R.G. Bristow, Chronic Hypoxia Decreases Synthesis of Homologous Recombination Proteins to Offset Chemoresistance and Radioresistance, Cancer Res. 68 (2008) 605–614, https://doi.org/10.1158/0008-5472.CAN-07-5472.
[22] A. Sahu, W.I. Choi, G. Tae, Recent progress in the design of hypoxia-specific nano drug delivery systems for cancer therapy, Adv. Ther. (Weinh) 1 (2018) 1800026, https://doi.org/10.1002/adtp.201800026.
[23] Y. Liu, Y. Jiang, M. Zhang, Z. Tang, M. He, W. Bu, Modulating hypoxia via nanomaterials chemistry for efficient treatment of solid tumors, Acc. Chem. Res. 51 (2018) 2502–2511, https://doi.org/10.1021/acs.accounts.8b00214.
[24] H. Lin, Y. Chen, J. Shi, Nanoparticle-triggered in situ catalytic chemical reactions for tumour-specific therapy, Chem. Soc. Rev. 47 (2018) 1938–1958, https://doi.org/10.1039/C7CS00471K.
[25] L. Zhao, C. Fu, L. Tan, T. Li, H. Zhong, X. Meng, Advanced nanotechnology for hypoxia-associated antitumor therapy, Nanoscale 12 (2020) 2855–2874, https://doi.org/10.1039/C9NR09071A.
[26] Y. Wan, L. Fu, C. Li, J. Lin, P. Huang, Conquering the Hypoxia Limitation for Photodynamic Therapy, Adv. Mater. 33 (2021) 2103978, https://doi.org/10.1002/adma.202103978.
[27] H. Wang, J. Li, Y. Wang, X. Gong, X. Xu, J. Wang, Y. Li, X. Sha, Z. Zhang, Nanoparticles-mediated reoxygenation strategy relieves tumor hypoxia for enhanced cancer therapy, J. Control. Release 319 (2020) 25–45, https://doi.org/10.1016/j.jconrel.2019.12.028.
[28] T.W. Secomb, R. Hsu, E.T. Ong, J.F. Gross, M.W. Dewhirst, Analysis of the effects of oxygen supply and demand on hypoxic fraction in tumors, Acta Oncol. 34 (1995) 313–316, https://doi.org/10.3109/02841869509093981.
[29] S. Shiva, P.S. Brookes, R.P. Patel, P.G. Anderson, V.M. Darley-Usmar, Nitric oxide partitioning into mitochondrial membranes and the control of respiration at cytochrome *c* oxidase, Proc. Natl. Acad. Sci. U.S.A. 98 (2001) 7212–7217, https://doi.org/10.1073/pnas.131128898.
[30] K.C. Valkenburg, A.E. De Groot, K.J. Pienta, Targeting the tumour stroma to improve cancer therapy, Nat. Rev. Clin. Oncol. 15 (2018) 366–381, https://doi.org/10.1038/s41571-018-0007-1.
[31] A.D. Theocharis, S.S. Skandalis, C. Gialeli, N.K. Karamanos, Extracellular matrix structure, Adv. Drug Deliv. Rev. 97 (2016) 4–27, https://doi.org/10.1016/j.addr.2015.11.001.
[32] Q. Chen, G. Liu, S. Liu, H. Su, Y. Wang, J. Li, C. Luo, Remodeling the tumor microenvironment with emerging nanotherapeutics, Trends Pharmacol. Sci. 39 (2018) 59–74, https://doi.org/10.1016/j.tips.2017.10.009.
[33] X. Chen, R. Jin, Q. Jiang, Q. Bi, T. He, X. Song, M. Barz, H. Ai, X. Shuai, Y. Nie, Delivery of siHIF-1α to reconstruct tumor normoxic microenvironment for effective chemotherapeutic and photodynamic anticancer treatments, Small 17 (2021) 2100609, https://doi.org/10.1002/smll.202100609.
[34] X. Zhao, J. Liu, J. Fan, H. Chao, X. Peng, Recent progress in photosensitizers for overcoming the challenges of photodynamic therapy: from molecular design to application, Chem. Soc. Rev. 50 (2021) 4185–4219, https://doi.org/10.1039/D0CS00173B.
[35] M.S. Baptista, G.L. Indig, Effect of BSA binding on photophysical and photochemical properties of triarylmethane dyes, J. Phys. Chem. B. 102 (1998) 4678–4688, https://doi.org/10.1021/jp981185n.
[36] M. Gao, Z. Wang, H. Zheng, L. Wang, S. Xu, X. Liu, W. Li, Y. Pan, W. Wang, X. Cai, R. Wu, X. Gao, R. Li, Two-dimensional tin selenide (snse) nanosheets capable of mimicking key dehydrogenases in cellular metabolism, Angew. Chem. Int. Ed. 59 (2020) 3618–3623, https://doi.org/10.1002/anie.201913035.
[37] W. Fan, W. Bu, B. Shen, Q. He, Z. Cui, Y. Liu, X. Zheng, K. Zhao, J. Shi, Intelligent MnO_2 nanosheets anchored with upconversion nanoprobes for concurrent pH-/H_2O_2-responsive UCL imaging and oxygen-elevated synergetic therapy, Adv. Mater. 27 (2015) 4155–4161, https://doi.org/10.1002/adma.201405141.
[38] C. Chu, H. Lin, H. Liu, X. Wang, J. Wang, P. Zhang, H. Gao, C. Huang, Y. Zeng, Y. Tan, G. Liu, X. Chen, Tumor microenvironment-triggered supramolecular system as an in situ nanotheranostic generator for cancer phototherapy, Adv. Mater. 29 (2017) 1605928, https://doi.org/10.1002/adma.201605928.
[39] X. Liu, J. Li, A. Zitolo, M. Gao, J. Jiang, X. Geng, Q. Xie, D. Wu, H. Zheng, X. Cai, J. Lu, F. Jaouen, R. Li, Doped graphene to mimic the bacterial NADH oxidase for one-step NAD^+ supplementation in mammals, J. Am. Chem. Soc. 145 (2023) 3108–3120, https://doi.org/10.1021/jacs.2c12336.
[40] E.S.G. Barron, The catalytic effect of methylene blue on the oxygen consumption of tumors and normal tissues, J. Exp. Med. 52 (1930) 447–456, https://doi.org/10.1084/jem.52.3.447.
[41] W.B. Wendel, The control of methemoglobinemia with methylene blue 12, J. Clin. Invest. 18 (1939) 179–185, https://doi.org/10.1172/JCI101033.
[42] W.B. Wendel, The mechanism of the antidotal action of methylene blue in cyanide poisoning, Science 80 (1934) 381–382, https://doi.org/10.1126/science.80.2078.381.
[43] M.M. Brooks, The mechanism of methylene blue action on blood, Science 80 (1934) 15–16, https://doi.org/10.1126/science.80.2062.15.b.
[44] M.M. Brooks, Methylene blue as antidote for cyanide and carbon monoxide poisoning, JAMa 100 (1933) 59, https://doi.org/10.1001/jama.1933.02740010061028.
[45] G. Hong, A.L. Antaris, H. Dai, Near-infrared fluorophores for biomedical imaging, Nat. Biomed. Eng. 1 (2017), https://doi.org/10.1038/s41551-016-0010, 0010.
[46] J. Park, P. Mroz, M.R. Hamblin, A.N. Yaroslavsky, Dye-enhanced multimodal confocal microscopy for noninvasive detection of skin cancers in mouse models, J. Biomed. Opt. 15 (2010) 026023, https://doi.org/10.1117/1.3394301.
[47] J. Chen, T.C. Cesario, P.M. Rentzepis, Effect of pH on methylene blue transient states and kinetics and bacteria photoinactivation, J. Phys. Chem. A. 115 (2011) 2702–2707, https://doi.org/10.1021/jp110215g.
[48] J.P. Tardivo, A. Del Giglio, L.H.C. Paschoal, A.S. Ito, M.S. Baptista, Treatment of melanoma lesions using methylene blue and RL50 light source, Photodiagn. Photodyn. Ther. 1 (2004) 345–346, https://doi.org/10.1016/S1572-1000(05)00005-0.
[49] J.P. Tardivo, A. Del Giglio, C.S. De Oliveira, D.S. Gabrielli, H.C. Junqueira, D. B. Tada, D. Severino, R. De Fátima Turchiello, M.S. Baptista, Methylene blue in photodynamic therapy: from basic mechanisms to clinical applications, Photodiagn. Photodyn. Ther. 2 (2005) 175–191, https://doi.org/10.1016/S1572-1000(05)00097-9.
[50] K. Orth, D. Russ, G. Beck, A. Rück, H.G. Beger, Photochemotherapy of experimental colonic tumours with intra-tumorally applied methylene blue, Langenbeck's Arch. Surg. 383 (1998) 276–281, https://doi.org/10.1007/s004230050132.
[51] M. Wainwright, K.B. Crossley, Methylene blue - a therapeutic dye for all seasons? J. Chemother. 14 (2002) 431–443, https://doi.org/10.1179/joc.2002.14.5.431.
[52] K. König, V. Bockhorn, W. Dietel, H. Schubert, Photochemotherapy of animal tumors with the photosensitizer methylene blue using a krypton laser, J. Cancer Res. Clin. Oncol. 113 (1987) 301–303, https://doi.org/10.1007/BF00396390.
[53] R.F. Tepaev, V.A. Vishnevskiy, S.A. Kuzin, I.V. Sergey, O.B. Gordeeva, A.V. Pytal, N.N. Murashkin, Benzocaine-induced methemoglobinemia. A clinical case, Pediatr. Farmakol. 15 (2018) 396–401, https://doi.org/10.15690/pf.v15i5.1962.
[54] M.I. Herman, P.A. Chyka, A.Y. Butler, S.E. Rieger, Methylene blue by intraosseous infusion for methemoglobinemia, Ann. Emerg. Med. 33 (1999) 111–113, https://doi.org/10.1016/s0196-0644(99)70427-0.
[55] R.E. Tranquada, Intravenous methylene blue in the therapy of lactic acidosis, Arch. Intern. Med. 114 (1964) 13, https://doi.org/10.1001/archinte.1964.03860070059003.
[56] A. Coronel, J. Catalán-Toledo, H. Fernández-Jaramillo, P. Godoy-Martínez, M. E. Flores, I. Moreno-Villoslada, Photodynamic action of methylene blue subjected to aromatic-aromatic interactions with poly(sodium 4-styrenesulfonate) in solution and supported in solid, highly porous alginate sponges, DyesPigm. 147 (2017) 455–464, https://doi.org/10.1016/j.dyepig.2017.08.042.
[57] H.C. Junqueira, D. Severino, L.G. Dias, M.S. Gugliotti, M.S. Baptista, Modulation of methylene blue photochemical properties based on adsorption at aqueous micelle interfaces, Phys. Chem. Chem. Phys. 4 (2002) 2320–2328, https://doi.org/10.1039/b109753a.
[58] R.H. Schirmer, H. Adler, M. Pickhardt, E. Mandelkow, Lest we forget you — methylene blue …, Neurobiol. Aging 32 (2011) https://doi.org/10.1016/j.neurobiolaging.2010.12.012, 2325.e7-2325.e16.
[59] P.R. Ginimuge, S.D. Jyothi, Methylene blue: revisited, J. Anaesthesiol. Clin. Pharmacol. 26 (2010) 517–520.
[60] J.F.J. Engbersen, A. Koudijs, H.C. Van Der Plas, Reaction of NADH models with methylene blue, Recl. Trav. Chim. Pays-Bas. 104 (2010) 131–138, https://doi.org/10.1002/recl.19851040503.
[61] P. Sevcik, H.B. Dunford, Kinetics of the oxidation of NADH by methylene blue in a closed system, J. Phys. Chem. 95 (1991) 2411–2415, https://doi.org/10.1021/j100159a054.

[62] D.J. Wales, R.M. Parker, J.C. Gates, M.C. Grossel, P.G.R. Smith, An integrated bragg grating oxygen sensor using a hydrophobic sol-gel layer doped with an organic dye, in: 2011 Conference on Lasers and Electro-Optics Europe and 12th European Quantum Electronics Conference (CLEO EUROPE/EQEC), Munich, Germany, IEEE, 2011, p. 1, https://doi.org/10.1109/CLEOE.2011.5943057.
[63] M. Oz, D.E. Lorke, M. Hasan, G.A. Petroianu, Cellular and molecular actions of methylene blue in the nervous system, Med. Res. Rev. 31 (2011) 93–117, https://doi.org/10.1002/med.20177.
[64] K. Buchholz, R.H. Schirmer, J.K. Eubel, M.B. Akoachere, T. Dandekar, K. Becker, S. Gromer, Interactions of methylene blue with human disulfide reductases and their orthologues from *Plasmodium falciparum*, Antimicrob. Agents Chemother 52 (2008) 183–191, https://doi.org/10.1128/AAC.00773-07.
[65] H. Atamna, A. Nguyen, C. Schultz, K. Boyle, J. Newberry, H. Kato, B.N. Ames, Methylene blue delays cellular senescence and enhances key mitochondrial biochemical pathways, FASEB J. 22 (2008) 703–712, https://doi.org/10.1096/fj.07-9610com.
[66] H. Atamna, R. Kumar, Protective role of methylene blue in Alzheimer's disease via mitochondria and cytochrome c oxidase, JAD 20 (2010) S439–S452, https://doi.org/10.3233/JAD-2010-100414.
[67] G.Roy Choudhury, A. Winters, R.M. Rich, M.-G. Ryou, Z. Gryczynski, F. Yuan, S.-H. Yang, R. Liu, Methylene blue protects astrocytes against glucose oxygen deprivation by improving cellular respiration, PLoS ONE 10 (2015) e0123096, https://doi.org/10.1371/journal.pone.0123096.
[68] K.K. Lee, U.A. Boelsterli, Bypassing the compromised mitochondrial electron transport with methylene blue alleviates efavirenz/isoniazid-induced oxidant stress and mitochondria-mediated cell death in mouse hepatocytes, Redox. Biol. 2 (2014) 599–609, https://doi.org/10.1016/j.redox.2014.03.003.
[69] P. Haouzi, M. Gueguinou, T. Sonobe, A. Judenherc-Haouzi, N. Tubbs, M. Trebak, J. Cheung, F. Bouillaud, Revisiting the physiological effects of methylene blue as a treatment of cyanide intoxication, Clin. Toxicol. 56 (2018) 828–840, https://doi.org/10.1080/15563650.2018.1429615.
[70] F. Bouillaud, C. Ransy, M. Moreau, J. Benhaim, A. Lombès, P. Haouzi, Methylene blue induced O2 consumption is not dependent on mitochondrial oxidative phosphorylation: implications for salvage pathways during acute mitochondrial poisoning, Respir. Physiol. Neurobiol. 304 (2022) 103939, https://doi.org/10.1016/j.resp.2022.103939.
[71] A.A. Stratonnikov, V.B. Loschenov, Evaluation of blood oxygen saturation in vivo from diffuse reflectance spectra, J. Biomed. Opt. 6 (2001) 457, https://doi.org/10.1117/1.1411979.
[72] S. Kalinina, C. Freymueller, N. Naskar, B. von Einem, K. Reess, R. Sroka, A. Rueck, Bioenergetic alterations of metabolic redox coenzymes as NADH, FAD and FMN by means of fluorescence lifetime imaging techniques, Int. J. Mol. Sci. 22 (2021) 5952, https://doi.org/10.3390/ijms22115952.
[73] P.M. Schaefer, S. Kalinina, A. Rueck, C.A.F. Von Arnim, B. Von Einem, NADH autofluorescence—a marker on its way to boost bioenergetic research, Cytometry Pt A. 95 (2019) 34–46, https://doi.org/10.1002/cyto.a.23597.
[74] M.H. Nisancioglu, C. Betsholtz, G. Genové, The absence of pericytes does not increase the sensitivity of tumor vasculature to vascular endothelial growth factor-a blockade, Cancer Res. 70 (2010) 5109–5115, https://doi.org/10.1158/0008-5472.CAN-09-4245.
[75] F. Shojaei, X. Wu, A.K. Malik, C. Zhong, M.E. Baldwin, S. Schanz, G. Fuh, H.-P. Gerber, N. Ferrara, Tumor refractoriness to anti-VEGF treatment is mediated by CD11b+Gr1+ myeloid cells, Nat. Biotechnol. 25 (2007) 911–920, https://doi.org/10.1038/nbt1323.
[76] J. Clifton, J.B. Leikin, et al., Methylene blue, in: J. Brent, K. Burkhart, P. Dargan, B. Hatten, B. Megarbane, R. Palmer, et al. (Eds.), Critical Care Toxicology, Springer International Publishing, Cham, 2017, pp. 2867–2878, https://doi.org/10.1007/978-3-319-17900-1_161.
[77] U. Hariharan, R. Sood, A. Choudhury, R. Garg, J. Kaur, Oxygen desaturation following methylene blue injection: not always spurious, Saudi. J. Anaesth. 5 (2011) 113, https://doi.org/10.4103/1658-354X.76471.
[78] A.J.C. Mittnacht, G.W. Fischer, D.L. Reich, Methylene blue administration is associated with decreased cerebral oximetry values, Anesth. Analg. 105 (2007) 549–550, https://doi.org/10.1213/01.ane.0000265695.72785.9d.
[79] H.J. Woehlck, M.T. Zundel, Characterization of the rapid drop in pulse oximetry reading after intraoperative administration of methylene blue in open thoracoabdominal aortic repairs, Anesth. Analg. 130 (2020) e179, https://doi.org/10.1213/ANE.0000000000004756.